Nuclear Instruments and Methods in Physics Research B 358 (2015) 32–37

Contents lists available at ScienceDirect

Nuclear Instruments and Methods in Physics Research B

journal homepage: www.elsevier.com/locate/nimb

Investigation of photoneutron and capture gamma-ray production in Pb and W under irradiation from ^{16}N decay radiation

Jeremiah Monari Kebwaro, Yaolin Zhao, Chaohui He *

School of Nuclear Science and Technology, Xian Jiaotong University, Xian, Shaanxi 710049, China

ARTICLE INFO

Article history:
Received 12 January 2015
Received in revised form 10 May 2015
Accepted 12 May 2015
Available online 25 May 2015

Keywords:
Photonuclear reactions
Radiative capture
Lead and tungsten
^{16}N decay radiation
Monte Carlo calculation

ABSTRACT

Lead and tungsten are potential alternative materials for shielding reactor ex-core components with high ^{16}N activity when available space limits application of concrete. Since the two materials are vulnerable to photonuclear reactions, the nature and intensity of the secondary radiation resulting from (γ,n) and (n,γ) reactions when ^{16}N decay radiation interact with these materials need to be well known for effective shielding design. In this study the MCNP code was used to calculate the photoneutron and capture gamma-ray spectra in the two materials when irradiated by ^{16}N decay radiation. It was observed that some of the photoneutrons generated in the two materials lie in the low-energy range which is considered optimum for (n,γ) reactions. Lead is more transparent to the photoneutrons when compared to tungsten. The calculations also revealed that the bremsstrahlung generated by the beta spectrum was not sufficient to trigger any additional photoneutrons. Both energetic and less energetic capture gamma-rays are observed when photoneutrons interact with nuclei of the two materials. Depending on the strength of the ^{16}N source term, the secondary radiation could affect the effectiveness of the shield and need to be considered during design.

1. Introduction

Neutron activation of ^{16}O in commercial or research reactors employing pure water or carbon dioxide as a coolant generate large quantities of ^{16}N, a short-lived radioactive isotope that emits energetic gamma-rays during decay. This isotope is transported to components located outside the core raising dose levels around them during reactor operation. Some of the reactors whose ex-core components would contain high levels of ^{16}N include boiling water reactors (BWR) [1], gas cooled reactors, pool in tank research reactors [2] and the proposed supercritical water cooled reactors (SCWR) [3]. It is a requirement that ex-core components with large quantities of this isotope should be entombed in a heavy shield to protect personnel during reactor operation [2,4,5]. Sometimes a concrete shield of up to 1 m in thickness is imposed around these components to ensure the area is accessible [5]. However as smaller modular reactors are being developed [6,7], space for constructing an enormous shield might be limited hence the need for lean but effective shielding around ex-core components. Lead and tungsten could be the alternative materials for shielding ^{16}N gamma rays when space is premium considering their high atomic numbers and mass densities. However the photoneutron threshold energies of some isotopes of these two elements [8] are lower than the energy of some ^{16}N decay photons which implies vulnerability to photoneutron production. Furthermore, the energy spectrum of ^{16}N beta particles that spans up to 10.4 MeV could also generate a bremsstrahlung spectrum capable of triggering photonuclear reactions. The additional dose created by these photoneutrons and the capture gamma-rays from (n,γ) reactions should be taken into account during shielding design for an effective shield. Therefore the nature and characteristics of these secondary radiations will be of crucial importance to the shielding engineer. Although evidence of photoneutron production in high Z elements has been reported in medical, port cargo inspection and research facilities [9–12] the possibility of such reactions in the context of irradiation from ^{16}N decay photons in the reactor coolant circuit is currently speculative [13] since quantitative evidence of such reactions has not been reported. The aim of this study was to determine the characteristics of the photoneutron and radiative capture spectra generated in lead and tungsten when they are irradiated by ^{16}N decay radiation (gamma-rays and beta particles).

2. Theoretical background

Photoneutrons are occasionally produced when incident photon energy exceeds the neutron separation energy of the target

* Corresponding author. Tel./fax: +86 29 82665915.
E-mail address: hechaohui@mail.xjtu.edu.cn (C. He).

http://dx.doi.org/10.1016/j.nimb.2015.05.012
0168-583X/

Table 1
photo-neutron threshold energy of major isotopes of lead and Tungsten [8].

Isotope	Natural abundance (%)	Photo-neutron threshold energy (MeV)
^{206}Pb	24.1	8.09
^{207}Pb	22.10	6.74
^{208}Pb	52.40	7.37
^{182}W	26.30	8.07
^{183}W	14.28	6.19
^{184}W	30.7	7.41
^{186}W	28.6	7.19

nucleus. The neutron separation energy (Sn) of the atomic nucleus is the threshold energy that has to be overcome for this reaction to take place. Threshold energies for stable isotopes of most elements are in the range $E > 10$ MeV but a few isotopes of some elements have threshold energies below 10 MeV [8]. As shown in Table 1, isotopes of lead and tungsten are among the few isotopes with low photoneutron threshold energies. The giant dipole resonance (GDR) is the predominant mechanism responsible for this reaction when the irradiating photons are in the low-energy range [12,14]. In high Z nuclei, the reaction is assumed to proceed in two overlapping steps. First a short-lived excited state of the parent nucleus is formed immediately the gamma-ray is absorbed. While this state lives, energy is shared among the nucleons until one or more nucleons are able to escape. The cross-section for this reaction is different for different isotopes [11] and is a function of incident photon energy [15] as shown in Eq. (1).

$$\sigma_{\mathrm{INT}} = \int_{E\text{-th}}^{E_{\max}} \sigma(E)dE \tag{1}$$

where σ_{INT} is the integrated cross-section, E-th is the photoneutron threshold energy and $E_{\max}$ is the upper energy limit.

The generated neutrons may undergo several interactions with the target nuclei resulting in emission of secondary radiations. Among these reactions, radiative capture (n,γ) is the most probable for low-energy neutrons and is of interest in shielding because several capture gamma rays are emitted. Eq. (2) can be used to express the intensity of gamma-rays emitted from radiative capture reactions [16].

$$I_\gamma = \iint \frac{\mu(r)}{M} N_A \sigma_\gamma(E_{\mathrm{n}})\phi(E_{\mathrm{n}}, r)dEdr \tag{2}$$

where $\mu(r)$ is the mass density of the target element expressed as a function of position (in case of inhomogeneity in density distribution), M is the relative atomic mass of the element, N_A is the Avogadro's constant, $\sigma_\gamma(E_{\mathrm{n}})$ is the energy dependent gamma-ray production cross-section and $\phi(E_{\mathrm{n}},r)$ is the energy and spatial dependent neutron flux. Since the kinetic energy of particles is a function of velocity, the capture cross-section is also expressed as a function of neutron velocity as shown in Eq. (3) [17].

$$\sigma_{\mathrm{eff}} = \frac{1}{v_0}\int_0^\infty \rho(v)\sigma_\gamma(v)vdv \tag{3}$$

where σ_{eff} is the effective capture cross-section and $\sigma(v)$ is the energy dependent cross-section while v_0 is the most probable velocity for thermal neutrons which is approximately 2200 m/s.

Radiative capture cross-sections for some isotopes of lead and tungsten obtained from ENDF/B-VII are shown in Fig. 1.

3. Monte-Carlo calculations

Monte Carlo N-particle code (MCNP) was used to calculate the flux and spectra of the secondary radiations. The MCNP model for photoneutron calculation consists of a simple sphere of radius 30 cm partitioned into five cells based on radial distance from the center of the sphere. The material of the innermost cell is stainless steel while all the peripheral cells are composed of the material under investigation (lead or tungsten). This simple arrangement was adopted to mimic a practical situation where ^{16}N is normally enclosed in a steel pipe or casing and the shield is constructed outside. The radius of the stainless steel inner cell was 1 cm, which is approximately the thickness of high-pressure turbine casings in commercial reactors. The source was located at the center of the sphere in all calculations. Fig. 2 shows the geometry of the MCNP model used in the calculations.

To calculate the flux and spectrum of photoneutron crossing the surfaces of the sphere, the gamma-ray spectrum of ^{16}N (Table 2) was declared as the source and the problem run in neutron photon mode (n,p). The F2 tally, which calculates average flux across a surface, was used to estimate the neutron flux across the surfaces. In addition, the tally card was tagged with an energy divider card (E_n) to determine the spectrum of neutrons crossing each surface. The MPN and the photonuclear physics cards were clearly stated in the input file, while ensuring that the MPN card for stainless steel remained zero to avoid photonuclear reactions between the 8.87 MeV photon (from ^{16}N decay) and ^{57}Fe nuclei whose threshold energy is 7.65 MeV [8].

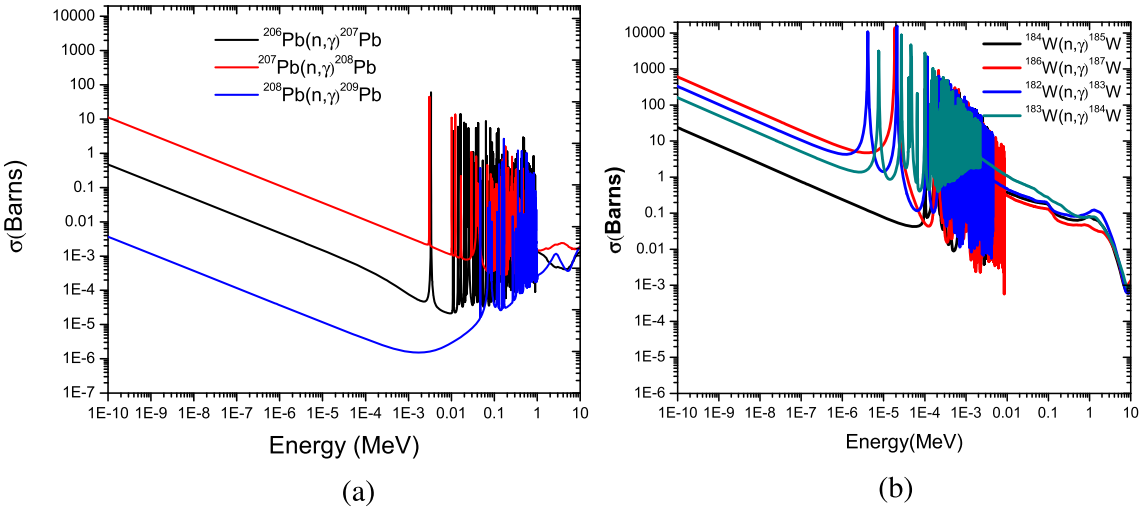

Fig. 1. Radiative capture reaction cross-sections for some isotopes of lead and tungsten from ENDF-B/VII [18]. (a) Shows lead isotopes while (b) shows tungsten isotopes.

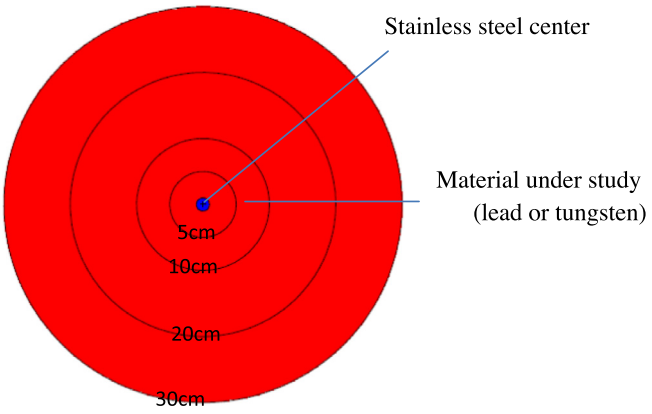

Fig. 2. The spherical geometry modeled in MCNP for photoneutron calculation. The dimensions represent the radii of tally surfaces. The photon source is located at the center of the sphere.

Table 2
Energy spectrum of ^{16}N decay photons obtained from IAEA data centre (https://www-nds.iaea.org/relnsd/vcharthtml/VChartHTML.html). The Energy of the photons has been rounded off to two decimal places.

Gamma-ray energy (MeV)	Emission probability
0.79	1.50E−08
0.87	2.10E−06
0.99	3.40E−05
1.07	1.50E−07
1.75	1.21E−03
1.95	3.80E−04
2.74	8.20E−03
2.82	1.30E−03
6.12	6.70E−01
6.92	3.80E−04
7.12	4.90E−02
8.87	7.60E−04

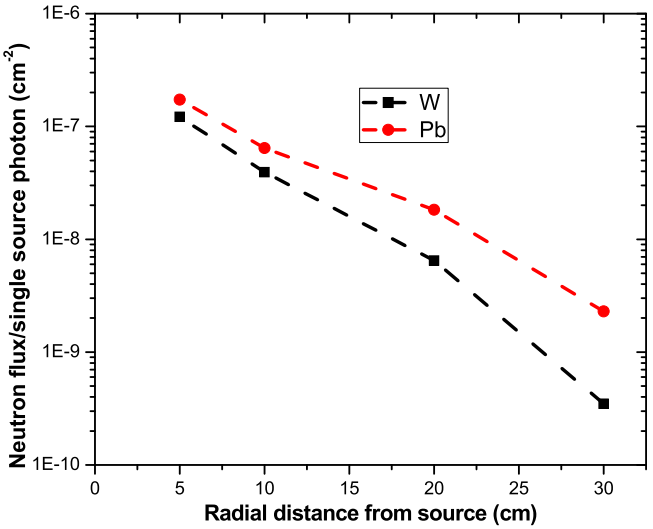

Fig. 3. Averaged photoneutron flux across the surfaces of the sphere calculated by MCNP. MCNP tallies are averaged over the number of source particles hence the flux in this figure represents the average contribution of a single source photon.

The radiative capture gamma-ray spectrum was calculated using the same geometry but with modifications on the source and material cards. The photoneutron spectrum tally obtained at the 5 cm radius surface (Fig. 2) in the above calculation was used as the neutron source placed at the center. The entire sphere was composed of the material under investigation (lead and tungsten). The problem was run in a neutron photon electron (n p e) mode to ensure all particles generated are accounted for. Since the main purpose of the calculation was to investigate the evidence of radiative capture and discriminate the photopeaks, tallies were only recorded in the second cell from the center using F4 card tagged with E_n card. The F4 card was preferred over F2 card to minimize chances of repeated counting at the surfaces due to back scattering.

To assess the contribution of ^{16}N beta particles to the photoneutron and capture spectrum another MCNP simulation was run with ^{16}N beta spectrum as the electron source in an n p e mode. The ^{16}N beta spectrum data from ICRP publication 107 [19] was used in the calculation. The geometry and tally cards that had been used for the photon source were retained in this new input file but another additional tally was used to record the bremsstrahlung spectrum in the second cell from the center.

The number of histories in each simulation was high enough (100 million particles history) to guarantee reliable statistics. Photonuclear cross-section data from the CNDC01u were used for tungsten isotopes while those from la150u were used for lead isotopes [8,20]. For other interaction processes, cross-sections from ENDF-B/VII [18] were used. Variance reduction techniques were also employed in the calculations to ensure the problem converges quickly.

4. Results and discussions

The average photoneutron flux densities across the surfaces of the sphere for both lead and tungsten calculated by MCNP are shown in Fig. 3. It can be observed that the neutron flux decreases gradually as the radial distance from the source increases mostly due to absorption in the materials. From the figure, it is also evident that the neutron flux is slightly higher in lead compared to Tungsten. This observation can be attributed to the differences in neutron reaction cross-sections of the isotopes of the two materials as shown in Fig. 1. The extent to which the photoneutron generated could influence shielding design will depend on the gamma source strength. For high ^{16}N activity, the dose from the neutrons could be significant enough to be factored in the shielding design considering the high quality factor allotted to neutrons [21].

The calculated photoneutron spectra for the two materials are shown in Figs. 4 and 5 respectively. A critical look at the neutron spectrum in lead shows that majority of the neutrons fall in the $E < 0.5$ MeV energy range. This observation is mainly because the 7.12 MeV gamma-ray is the main contributor to the photonuclear reactions in the material considering its high intensity compared to 6.92 MeV and 8.87 MeV (Table 2). It is also important to note that the difference between the 7.12 MeV photon and the photoneutron threshold energy of ^{207}Pb (Table 1) is less than 0.5 MeV. The tail of the spectrum in the high-energy range is mainly caused by the 8.87 MeV photon that exceeds the photoneutron threshold energies of lead isotopes by a higher margin but its intensity is much lower than that of 7.12 MeV (Table 2). Another possible reason for the suppressed photoneutron intensity beyond 0.5 MeV could be resonant capture reactions since the resonance peaks in the (n,γ) excitation functions of lead isotopes lie within this range (Fig. 1). The difference in the intensity of the spectra at various radial distances is mainly due to loss of energy and eventual absorption of some neutrons as they travel in the material.

The photoneutron spectrum in tungsten (Fig. 5) does not show any tail for the energy range ($E \leqslant 1.0$ MeV) considered for neutron spectrum tallies. This observation is not surprising considering that the energy difference between the 7.12 MeV from ^{16}N and the photoneutron threshold energy of ^{183}W is almost 1 MeV. The enhanced

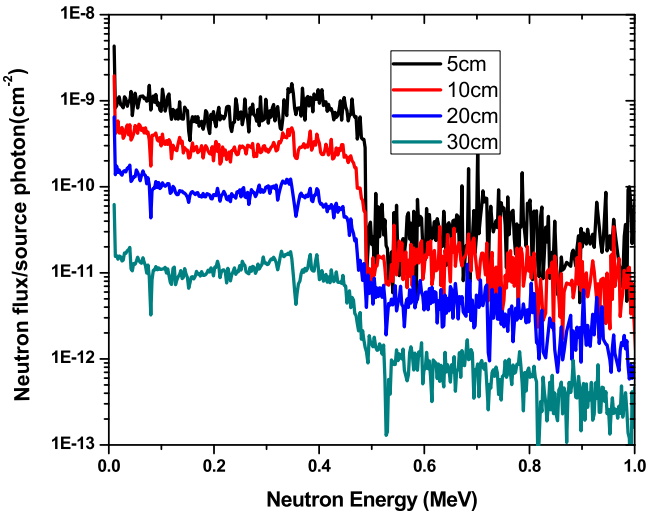

Fig. 4. Photoneutron spectrum in lead calculated by MCNP. The Tail beyond 0.5 MeV is due to the 8.87 MeV photon whose energy exceeds the threshold energy of lead isotopes by a large margin.

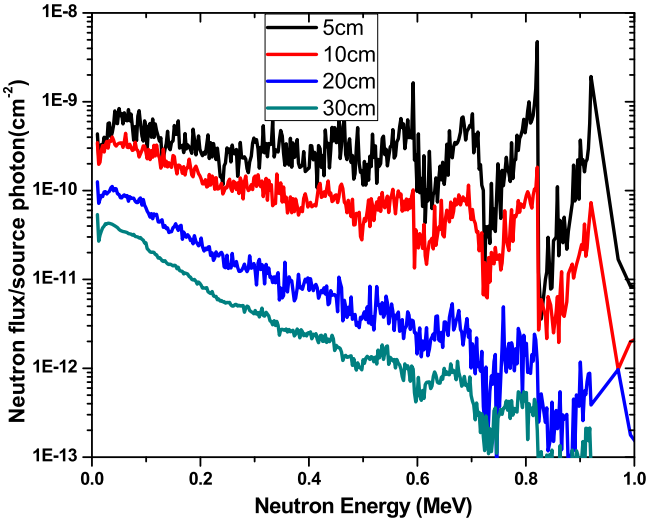

Fig. 5. Photoneutron spectrum in tungsten calculated by MCNP.

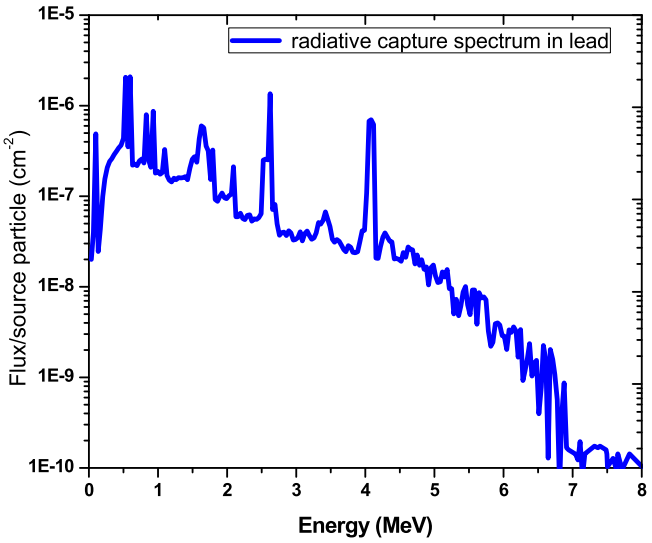

Fig. 6. Gamma-ray spectrum in lead resulting from (n,γ) reactions between lead nuclei and the generated photoneutrons.

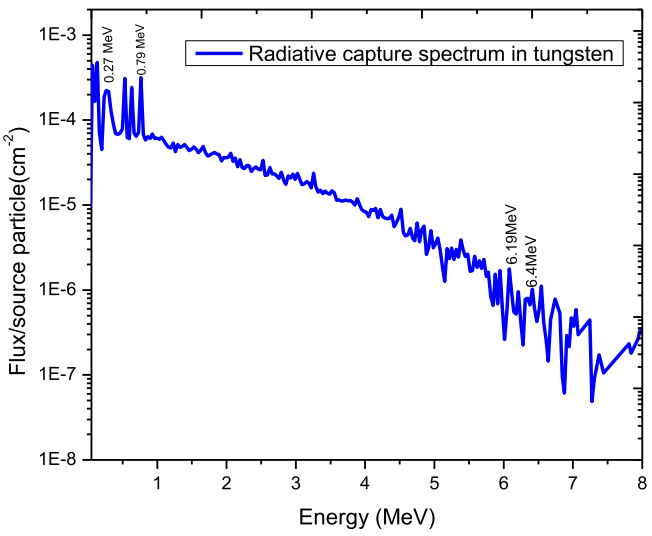

Fig. 7. Gamma-ray spectrum in tungsten resulting from (n,γ) reactions between tungsten nuclei and the generated photoneutrons.

intensity observed at some energy points between 0.6 MeV and 1 MeV could also be attributed to the contribution from the 8.87 MeV gamma-ray. Another important observation from the two figures (Figs. 4 and 5) is that some of the generated photoneutrons lie in the thermal and epithermal energy ranges where radiative capture reactions are known to thrive most [22–24].

The gamma-ray spectra generated in lead and tungsten due to (n,γ) reactions are shown in Figs. 6 and 7 respectively. The position of the photopeaks (photopeak energy) obtained in this calculation are consistent with experimental values reported in literature [17,25], confirming that the Monte Carlo calculation was correct. Some of the peaks are labeled in Fig. 7. Both energetic and less energetic photopeaks can be observed in the two materials. It was expected that the intensity of some energetic photopeaks in the two materials would be very high (especially beyond 6 MeV) but the simulation revealed otherwise. This would have happened probably because most neutrons escaped the tally region before thermalizing because thermal neutrons are the most responsible for energetic capture gamma-ray signatures. Although the energy of photoneutrons is generally low, it is only a small section of the spectrum that falls within the thermal-energy range. Hence for many slow neutron capture events to occur the neutrons in the higher section of the spectrum have to be moderated to thermal energies. Furthermore high Z nuclei are poor neutron moderators because of their low neutron scattering cross-sections thus many neutrons could travel long distances in the materials before attaining the thermal-energy range. Some limitations in the cross-section data might have also contributed to this phenomenon and parallel calculations using (n,γ) cross-section data from other files are necessary in future studies to ensure that large uncertainties in the cross-section data are not overlooked.

The gamma-rays could significantly contribute to the shielded dose especially if such capture reactions occur near the edge of the shield. There is therefore need to consider such events during shielding design.

No photoneutron flux was recorded when the beta spectrum was used as the source. This was mainly because the bremsstrahlung generated (Fig. 8) was not sufficient to trigger photonuclear reactions. The bremsstrahlung is dominated by low-energy

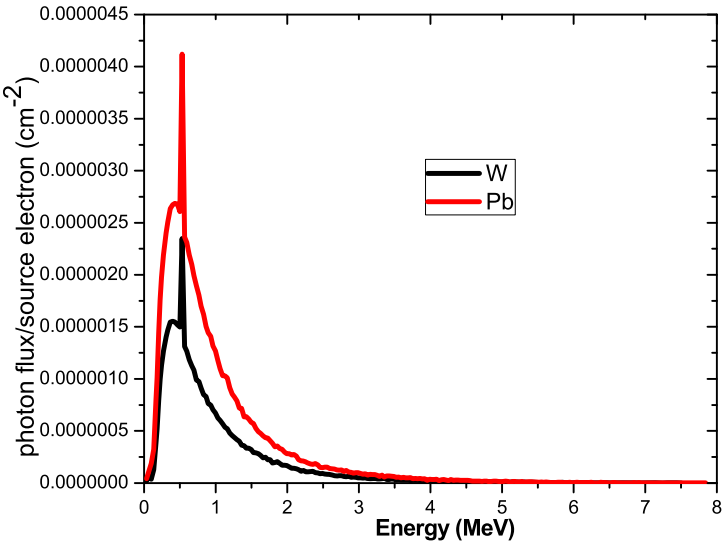

Fig. 8. Bremsstrahlung spectrum generated in lead and tungsten due to irradiation from beta particles. The tallies were recorded in the second cell from the center of the sphere.

photons with only a residual tail in the high-energy range similar to that of the ^{16}N beta spectrum where the intensity decreases with increase in energy with the lowest intensity being at the maximum energy [19]. The low intensity in the higher-energy range of the beta spectrum is due to the low probability for exclusive beta decay, which is responsible for the high-energy section of the spectrum as opposed to a higher probability for emission of mixed radiation (https://www-nds.iaea.org/relnsd/vcharthtml/VChartHTML.html).

From this study it is evident that ^{16}N decay photons can induce photoneutrons in Lead and Tungsten. Radiative capture reactions are also witnessed when the generated photoneutrons interact with the atomic nuclei. Depending on the strength of the source, the generated secondary radiation could lead to additional dose that could require intervention during shielding design considering the quality factors of these particles [21]. To ensure these materials efficiently shield ^{16}N with a very lean thickness, modification of some properties is necessary. The modification may include manufacture of metal foams and filling the voids with materials with high neutron absorption cross-section like borax or cadmium. Another alternative is to construct the shield in thin alternating layers.

5. Conclusion

MCNP code has been successfully used to investigate production of photoneutron and capture gamma-rays in lead and tungsten due to irradiation from ^{16}N decay radiation. The calculations show that the photoneutrons generated are capable of inducing radiative capture reactions in the materials. It is also observed that lead is more transparent to the photoneutrons compared to tungsten. Energetic primary gamma rays from slow neutron capture and low gamma-ray signatures are observed in the two materials. The bremsstrahlung spectrum that was generated by the ^{16}N beta particles was not sufficient enough to trigger photonuclear reactions in the materials. The extent to which the generated secondary radiation could affect the shielding design for reactor ex-core components containing ^{16}N will depend on the source strength. However some modifications of the material properties could be necessary for efficient ^{16}N shielding. The modification may include production of foams from the two materials and filling the voids with materials with high neutron absorption cross-section like borax.

References

[1] E. Ibe, H. Karasawa, S. Uchida, Radiation-chemistry of radioactive nitrogen species in BWR reactor cores, J. Nucl. Sci. Technol. 28 (4) (1991) 347–355, http://dx.doi.org/10.1080/18811248.1991.9731367.
[2] N. Sadeghi, Estimation of reactor power using ^{16}N production rate and its radiation risk assessment in Tehran Research Reactor (TRR), Nucl. Eng. Des. 240 (10) (2010) 3607–3610, http://dx.doi.org/10.1016/j.nucengdes.2010.06.029.
[3] T. Schulenberg, L.K.H. Leung, Y. Oka, Review of R&D for supercritical water cooled reactors, Prog. Nucl. Energy 77 (2014) 282–299, http://dx.doi.org/10.1016/j.pnucene.2014.02.021.
[4] USNRC. Consolidated guidance: 10CFR20-standards for protection against radiation *NUREG-1736*. Washington, DC, 2001.
[5] USEPA. Environmental Radiation protection for nuclear power operations. Proposed standards (40 CFR 190) Washington, D.C.: USEPA, 1976.
[6] IAEA. Status of Small Reactor Designs Without On-Site Refuelling. IAEA-TECDOC-1536, 2007.
[7] T. Abram, S. Ion, Generation-IV nuclear power: a review of the state of the science, Energy Policy 36 (12) (2008) 4323–4330, http://dx.doi.org/10.1016/j.enpol.2008.09.059.
[8] IAEA. Handbook on Photonuclear data. Cross-sections and Spectra. Vienna, 2000.
[9] P.J. Biggs, Evidence for photoneutron production in the lead shielding of a dedicated intra-operative electron only facility, Health Phys. 74 (1) (1998) 96–98.
[10] Y.H. Cho, J.H. Moon, C.S. Kang, Analysis of activation products generated from photoneutron capture reactions inside a linear accelerator used in a cargo inspection facility, Nucl. Instr. Meth. Phys. Res., Sect. B 265 (2) (2007) 615–620, http://dx.doi.org/10.1016/j.nimb.2007.10.006.
[11] F. Jallu, A. Lyoussi, E. Payan, H. Recroix, A. Mariani, G. Nurdin, Photoneutron production in tungsten, praseodymium, copper and berrylium by using high energy linear accelerator, Nucl. Instr. Meth. Phys. Res., Sect. B 55 (1999) 373–381.
[12] A. Naseri, A. Mesbahi, A review on photoneutrons characteristics in radiation therapy with high-energy photon beams, Rep. Pract. Oncol. Radiother. 15 (5) (2010) 138–144, http://dx.doi.org/10.1016/j.rpor.2010.08.003.
[13] J.M. Kebwaro, Y. Zhao, C. He, Evaluation of candidate materials for SCWR turbine and balance of plant shielding, Prog. Nucl. Energy 79 (2015) 136–141, http://dx.doi.org/10.1016/j.pnucene.2014.11.014.
[14] M.A. Saeed, Study of photoneutron cross-section: phenomenological approach to low mass targets, J. Al-Nahrain Univ. 12 (4) (2009) 113–122.
[15] A.V. Varlamov, V.V. Varlamov, D.S. Rudenko, M.E. Stepanov. Atlas of Giant Dipole Resonances. IAEA, INDC(NDS)-394, 1999.
[16] G.L. Molnar, Handbook of Prompt Gamma Activation Analysis with Neutron Beams, Kluwer Academic Publishers, Dordrecht, The Netherlands, 2004.
[17] IAEA. Database of prompt gamma rays from slow neutron capture for elemental analysis. STI/PUB/1263, 2007.

[18] M.B. Chadwick, M. Herman, P. Oblozinsky, M.E. Dunn, Y. Danon, A.C. Kahler, D.L. Smith, B. Pritychenko, G. Arbanas, R. Arcilla, R. Brewer, D.A. Brown, R. Capote, A.D. Carlson, Y.S. Cho, H. Derrien, K. Guber, G.M. Hale, S. Hoblit, S. Holloway, T.D. Johnson, T. Kawano, B.C. Kiedrowski, H. Kim, S. Kunieda, N.M. Larson, L. Leal, J.P. Lestone, R.C. Little, E.A. McCutchan, R.E. MacFarlane, M. MacInnes, C.M. Mattoon, R.D. McKnight, S.F. Mughabghab, G.P.A. Nobre, G. Palmiotti, A. Palumbo, M.T. Pigni, V.G. Pronyaev, R.O. Sayer, A.A. Sonzogni, N.C. Summers, P. Talou, I.J. Thompson, A. Trkov, R.L. Vogt, S.C. van der Marck, A. Wallner, M.C. White, D. Wiarda, P.C. Young, ENDF/B-VII.1 nuclear data for science and technology: cross sections, covariances, fission product yields and decay data, Nucl. Data Sheets 112 (12) (2011) 2887–2996, http://dx.doi.org/10.1016/j.nds.2011.11.002.

[19] ICRP. Nuclear Decay Data for Dosimetric Calculations. ICRP Publication 107. Annals of ICRP, 38(3), 2008.

[20] M.B. Chadwick, P.G. Young, S. Chiba, S.C. Frankle, G.M. Hale, H.G. Hughes, A.J. Koning, R.C. Little, R.E. MacFarlane, R.E. Prael, L.S. Waters, Cross-section evaluations to 150 MeV for accelerator-driven systems and implementation in MCNPX, Nucl. Sci. Eng. 131 (1999) 293–328.

[21] ICRP. The 1990 recommendations of the International Commission on Radiological protection. ICRP publication 60. Annals of the ICRP, 21(1–3), 1991.

[22] A.M. Hurst, R.B. Firestone, B.W. Sleaford, N.C. Summers, Z. Révay, L. Szentmiklósi, M.S. Basunia, T. Belgya, J.E. Escher, M. Krtička, Investigation of the tungsten isotopes via thermal neutron capture, Phys. Rev. C 89 (1) (2014) 014601–014606, http://dx.doi.org/10.1103/PhysRevC.89.014606.

[23] N. Van Do, P.D. Khue, K.T. Thanh, N.T. Hien, G. Kim, S. Yang, Y.-S. Cho, T.-Y. Song, Y.-O. Lee, S.G. Shin, M.-H. Cho, M.W. Lee, Thermal neutron capture cross section and resonance integral of the 139La(n,γ)140La reaction, Nucl. Instrum. Methods Phys. Res., Sect. B 335 (2014) 1–7, http://dx.doi.org/10.1016/j.nimb.2014.05.018.

[24] N.V. Do, P.D. Khue, K.T. Thanh, L.T. Son, G. Kim, Y.S. Lee, Y. Oh, H.-S. Lee, M.-H. Cho, I.S. Ko, W. Namkung, Thermal neutron cross-section and resonance integral of the 186W(n,γ)187W reaction, Nucl. Instr. Meth. Phys. Res., Sect. B 266 (6) (2008) 863–871, http://dx.doi.org/10.1016/j.nimb.2008.02.021.

[25] P.A. Treado, P.R. Chagnon, Neutron capture gamma-ray of the isotopes of tungsten, Nucl. Phys. 34 (1962) 623–627.